energies

Article

Performance Assessment of Closed-Brayton-Cycle and Thermoelectric Generator Combined Power Generation System Coupled with Hydrocarbon-Fueled Scramjet

Kunlin Cheng [1,2], Wuxing Jing [1], Jiahui Li [1] and Jiang Qin [1,2,*]

[1] Harbin Institute of Technology, Harbin 150001, China; chengkunlin@hit.edu.cn (K.C.); jingwuxing@hit.edu.cn (W.J.); lijiahui202305@163.com (J.L.)
[2] Chongqing Research Institute, Harbin Institute of Technology, Chongqing 401120, China
[*] Correspondence: qinjiang@hit.edu.cn

Abstract: Closed-Brayton-cycle (CBC) is a potential scheme to provide high-power electricity for hypersonic vehicles, but finite cold source onboard limits its power level. A thermoelectric generator (TEG) combined with CBC is a feasible power enhancement approach by extending the available temperature range of cold source. In this study, a performance assessment of the CBC-TEG combined power generation system coupled with hydrocarbon-fueled scramjet is performed to exhibit its possible operation characteristics and performance limitations on hypersonic vehicles. Results indicate that, at a fixed flight Mach number, a larger fuel equivalence ratio (φ) leads to a higher total electric power and CBC power but a lower TEG power. There are three limitations on the fuel equivalence ratio, TEG temperature difference, and combustion heat dissipation adjustment for the operation of CBC-TEG. The total power of CBC-TEG can be adjusted by φ, but the adjustable range becomes smaller at higher Ma. The electric quantity at unit fuel mass increases with φ, mainly due to the higher thermoelectric conversion efficiency. Moreover, the maximum value of the electric quantity at unit fuel mass for CBC-TEG reaches 277.0 kJ/kg, which is about 33.4% higher than that of standalone CBC.

Keywords: closed-Brayton-cycle; thermoelectric generator; hydrocarbon-fueled scramjet; hypersonic vehicle

check for updates

Citation: Cheng, K.; Jing, W.; Li, J.; Qin, J. Performance Assessment of Closed-Brayton-Cycle and Thermoelectric Generator Combined Power Generation System Coupled with Hydrocarbon-Fueled Scramjet. *Energies* **2023**, *16*, 7385. https://doi.org/10.3390/en16217385

Academic Editor: Mahmoud Bourouis

Received: 27 August 2023
Revised: 26 October 2023
Accepted: 30 October 2023
Published: 31 October 2023

1. Introduction

Hypersonic vehicles [1,2], the propulsion systems of which can be scramjets [3–6], combined cycle [7–10], or pre-cooled engines [11], are designed for commercial applications and military missions [12] in or across the atmosphere. These advanced vehicles demand a substantial and indispensable supply of electrical power to realize functions such as fuel feeding [13], radar detection, flight control [14], and potentially electromagnetic weapons [15]. The air-breathing hypersonic propulsion systems commonly have no rotating machinery for converting shaft power to electric energy, and meanwhile, the existing power generation devices, such as the auxiliary power unit (APU) [16] and ram air turbine (RAT) [17], have been proven unsuitable for hypersonic vehicles operating at high Mach numbers. Consequently, a diverse array of innovative technologies for onboard electricity generation has emerged in recent years. Magnetohydrodynamic (MHD) power generation has captured the attention of researchers, primarily due to its exceptional attributes including high power generation efficiency, rapid responsiveness, and seamless compatibility with scramjet systems [18]. Harada et al. [19] conducted a comprehensive series of experiments for scramjet-driven MHD power generation, culminating in the successful extraction of a reasonable output of electric power. Furthermore, numerical simulations, spanning both one and three dimensions, were executed to elucidate and expound upon the experimental findings. However, certain technical challenges persist prior to the practical application of MHD technology. Present superconductor materials remain reliant on cryogenic environments, with only liquid hydrogen being able to provide the requisite ultra-low temperatures within the context of hypersonic vehicles. Additionally, the ionization of airflow at low flight Mach numbers is so weak, making the noble metals as 'seed' necessary to enhance the ionization levels, which increases the cost dramatically.

In contrast, power generation devices based on thermal cycles have attained a higher degree of technical maturity, consequently garnering substantial interest among researchers. Building upon the foundation of a regenerative cooling system, a power generation concept centered around a fuel vapor turbine has been formulated. The inception of this concept can be attributed to Sforza, who initially introduced it as a Rankine cycle power generation plant [15]. The conceptual framework involves the utilization of high-pressure liquid fuel to absorb the heat generated by combustion within the combustor wall cooling channels, thereby transforming the fuel into vapor form. The ensuing steps encompass the division of the fuel vapor into a fuel injection stream and a bypass, with the latter being subjected to further superheating. This superheated bypass is subsequently employed to propel an electric generator through the agency of a fuel vapor turbine. The turbine's exhaust, once discharged, undergoes condensation back into a liquid state, with the fuel tank serving as the heat sink for this condensation process. However, this scheme is associated with two inherent drawbacks. Firstly, the mass flowrate of fuel vapor must be kept quite low to enable the condensation of the turbine exhaust, particularly when dealing with hydrocarbon fuel. This limitation substantially caps the achievable power output. Secondly, there exists the potential for heat transfer degradation within the wall cooling channels, especially when the fuel is in a subcritical state. This phenomenon exposes the system to significant risks of structural damage. To circumvent these limitations, Zhang put forth an open-cycle fuel-feeding and electricity supply system grounded in a hydrocarbon fuel vapor turbine. This alternative approach encompasses the development of a performance evaluation model for the fuel vapor turbine, employing the SRK (Soave–Redlich–Kwong) equation of state [13]. The outcomes of this evaluation indicate that the hydrocarbon fuel vapor turbine can indeed yield sufficient power to drive the fuel supply pump. This is attainable when specific conditions are met, such as a turbine expansion ratio of 2 and an isentropic enthalpy drop of over 100 kJ/kg at a turbine expansion ratio of 5 and an inlet temperature of 940 K. Furthermore, Li conducted an empirical study to assess the practical power generation performance of a fuel vapor turbine test system, culminating in the highest recorded output-specific work of 35 kJ/kg [20]. In summary, the power generation system based on a fuel vapor turbine holds several advantages in terms of its technological maturity, structural efficiency, and compact size. Nevertheless, its electric power output is constrained by the finite mass flowrate of fuel and the comparatively modest specific work of fuel vapor. Consequently, achieving high-power electricity generation through this approach remains a challenging proposition.

Owing to its compact size and high thermal efficiency, closed-Brayton-cycle (CBC) becomes another thermodynamic cycle suitable for onboard power generating. The working fluids employed within the CBC, such as helium–xenon mixtures [21] and supercritical carbon dioxide (S-CO_2) [22,23], exhibit superior performance in terms of heat transfer and heat–work conversion compared to common working fluids used in open cycles (typically air or fuel vapor). However, a critical limitation facing closed-Brayton-cycle systems is the finite availability of a cold source, a factor that significantly impacts their performance within the context of hypersonic vehicles. In our prior investigations, we engaged in the optimization of power output for an S-CO_2 CBC under conditions of finite cold source availability. This study involved a comparison between a simple recuperated layout and a recompressing layout in terms of specific power and thermal efficiency [24]. Results indicated that the recompressing layout had advantages in thermal efficiency, but the simple recuperated layout exhibited better electric power per unit mass flowrate of fuel, because the latter can utilize more cooling capacity of fuel. However, a significant performance degradation occurred for CBC under the finite cold source conditions because of the contradiction between the fuel cooling capacity and thermal efficiency.

Considering the limitation of single power generation systems, combined power generation systems are proposed to make better use of the cooling capacity of fuel. According to the Carnot theorem, a higher cold source temperature leads to a lower thermal efficiency under a constant heat source condition for thermodynamic cycles. Hence, it is a better choice to combine a thermal cycle-based generating system with a non-thermodynamic cycle power device. Thermoelectric generators (TEGs) [25,26], which are one of the non-thermodynamic cycle devices qualified to build combined power systems [27–29], have the potential to be combined with CBC on hypersonic vehicles. In previous research endeavors, a combined system that pairs a CBC with a TEG generator cooled by liquid methane has been proposed. In this configuration, the cold source is initially utilized by the CBC system and subsequently employed to cool the TEG, thus achieving a cascaded utilization of the cooling capacity inherent in the fuel. Theoretical investigations have substantiated that incorporating additional TEGs can notably enhance electric power output by broadening the available temperature range of the cold source in hypersonic vehicles. In fact, the CBC-TEG combined system achieved a remarkable 18.2% increase in power output compared to standalone CBC systems [30]. Hence, the combined CBC-TEG system emerges as a promising technological avenue for achieving high-power electricity generation objectives within the realm of hypersonic vehicles.

However, it is extremely difficult to obtain the actual performance of CBC-TEG if only analyzing the power plant itself because of the deep coupling relationship between the propulsion and power generation system for hypersonic vehicles. On the one hand, considering that the cold source of closed-cycle power generation system is the fuel of the propulsion system, as well as the propulsion system obviously has a higher priority, the cooling capacity of fuel actually depends on the demand of the combustion process. Meanwhile, the heat source of the power generation system comes from the heat dissipation from gas to engine walls, which means the quantity of heat available for electricity generation is also dependent on the combustion process of the engine. On the other hand, the cooling process of the power generation system has a significant influence on the combustion process through varying the injection state of the fuel. Thus, it is necessary to use an integrated design for the propulsion and power generation system of hypersonic vehicles.

This article focuses on the performance prediction of the combined CBC-TEG power generation system coupled with a hydrocarbon-fueled scramjet, in which CBC-TEG is involved in the cooling and power generation [31]. A liquid metal loop serves as the intermediary between the CBC-TEG and scramjet through transferring the combustor's heat dissipation to the combined power generation system. In this study, the performance evaluation model for the combined power generation system, the CBC power of which is optimized using the genetic algorithm under finite cold source conditions, is established, in which the energy balance among the scramjet combustor, wall cooling channels, closed-Brayton-cycle, and thermoelectric generator is achieved by iterations. Notably, the influence of the fuel equivalent ratio on power generation is dissected across various flight Mach numbers. Additionally, the operating range and performance boundary of the combined CBC-TEG power generation system are calculated to obtain its possible operation characteristics and performance limitations when CBC-TEG works in coordination with scramjet.

2. System Description

The configuration of the integrated power generation system, consisting of a closed-Brayton-cycle and thermoelectric generator in tandem with a hydrocarbon-fueled scramjet, is visually depicted in Figure 1. Within this configuration, liquid metal, specifically liquid sodium in this context, assumes dual roles. It serves as both the coolant for the combustor walls and the conduit for channeling the dissipated heat from combustion. This heat is subsequently directed towards both the heater of the CBC and the heating channel of the TEG. The hydrocarbon fuel undertakes a multifaceted role as well. It functions as the cold source, characterized by a cascading utilization approach. This entails its successive absorption of heat in the primary cooler of the CBC and the cooling channel of the TEG. Following this, the fuel finds its way into the combustor, contributing to the phenomenon of supersonic combustion. Thus, the scramjet emerges as the determinant of heat source parameters for the integrated power generation system, thereby influencing the fuel injection conditions for the entire arrangement. Conversely, the performance characteristics and behavior of the combined power generation system wield an influential role in shaping the fuel injection dynamics within the scramjet.

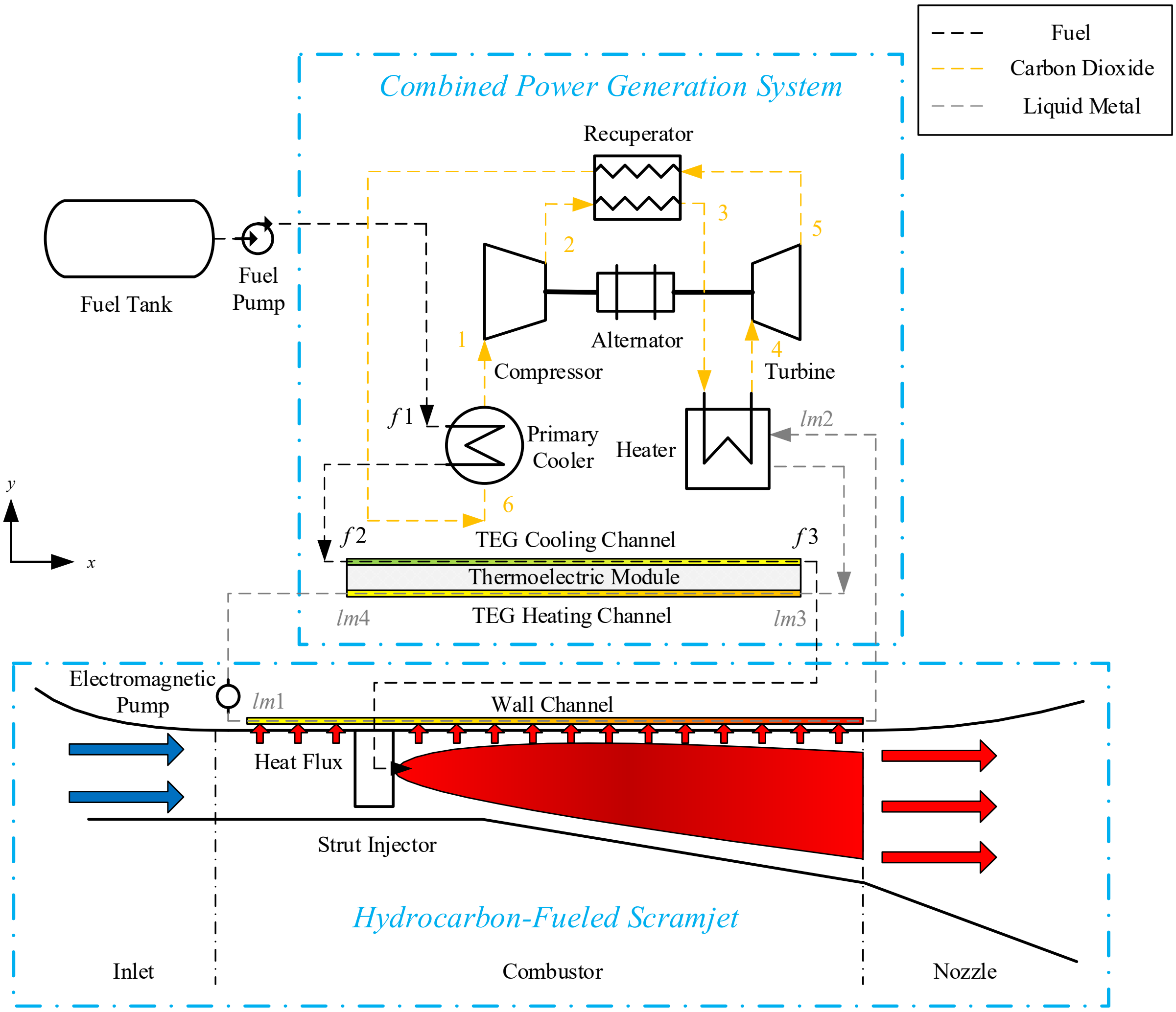

Figure 1. Sketch of combined CBC-TEG power generation system coupled with hydrocarbon-fueled scramjet.

The closed-Brayton-cycle power device employs a straightforward recuperated layout chosen for its benefits in terms of structural weight, system control, and electric power per unit mass flowrate of fuel. These advantages become particularly pronounced when operating under limited cold source conditions [24]. Given the significant temperature differential inherent in the thermoelectric generator, a three-stage thermoelectric module (TEM) is adopted to enhance the overall conversion efficiency.

3. Mathematic Modeling

The performance evaluation model for the combined CBC-TEG power generation system coupled with the hydrocarbon-fueled scramjet mainly consists of three key modules:

the power generation model, the supersonic combustion and heat dissipation model, and the flow and heat transfer model of the liquid metal and fuel. Due to the obvious distributed parameter characteristics of scramjets, the supersonic combustion and heat dissipation model, as well as the according flow and heat transfer model of liquid metal for combustor wall cooling, are established in quasi-one-dimension. To exhibit the significant temperature variation in the TEG heating and cooling channels, the flow and heat transfer processes of the liquid metal and fuel for TEG channels are also described by quasi-one-dimensional models. Moreover, considering the great iteration number in the power optimization with finite cold source, the CBC model is developed in zero-dimension. In this way, a balance between the computation speed and calculation accuracy is achieved in the modeling for the combined CBC-TEG power generation system coupled with hydrocarbon-fueled scramjet.

3.1. Power Generation Model

The closed-Brayton-cycle model is formulated in a zero-dimensional framework to expedite computation. The isentropic efficiency of the compressor is represented as follows:

$$\eta_C = \frac{h_{2s} - h_1}{h_2 - h_1} \tag{1}$$

where h is the enthalpy of carbon dioxide.

Taking into account the higher specific heat of carbon dioxide at the cold side compared to that at the hot side, the effectiveness of the recuperator can be expressed as follows:

$$\varepsilon_{REC} = \frac{h_5 - h_6}{h_5 - h(T_2, p_6)} \tag{2}$$

The isentropic efficiency of the turbine is defined as follows:

$$\eta_T = \frac{h_4 - h_5}{h_4 - h_{5s}} \tag{3}$$

The pressure ratio of the turbine relies on the pressure ratio of the compressor and the relative pressure loss coefficients of the three heat exchangers.

$$\pi_T = \frac{p_4}{p_5} = \pi_C \prod_{i=1}^{n} (1 - \xi_i) \tag{4}$$

The electric power output of the simple recuperated layout with a finite cold source is determined by the following expression:

$$P_{CBC} = \dot{m}_{CO_2}(w_T - w_C)\eta_G = \dot{m}_f \frac{h_{f2} - h_{f1}}{h_6 - h_1}[(h_4 - h_5) - (h_2 - h_1)]\eta_G \tag{5}$$

where w_T and w_C represent the specific work of the turbine and compressor, respectively, and η_G signifies the efficiency of the generator.

For a thermoelectric generator, the convective heat transfer rate between liquid metal and the heating channel wall is equal to the heat transfer rate on the hot side of the ceramic plate:

$$A_{hc} h_{c_{hc}}^{i} \left[T_{fh}(i) - T_{wh}(i)\right] = K_{cp_i}^{1} \left[T_{wh}(i) - T_{jh}^{1}(i)\right] \tag{6}$$

where h_c stands for the convection heat transfer coefficient, and K_{cp} represents the thermal conductance of the insulated ceramic plates ($K_{cp} = \lambda_{cp} A_{cp} / \theta_{cp}$).

Similarly, the heat transfer rate between the fuel and the cooling channel wall equals the heat transfer rate occurring on the cold side of the ceramic plate:

$$K_{cp_i}^{n+1} \left[T_{jc}^{n}(i) - T_{wc}(i)\right] = A_{cc} h_{c_{cc}}^{i} \left[T_{wc}(i) - T_{fc}(i)\right] \tag{7}$$

By combining the heat transfer equations, the temperatures of the junctions and channel walls within a three-stage thermoelectric module can be presented in matrix form as demonstrated below.

$$B \cdot T = C \tag{8}$$

Matrix B, wherein identical elements have been consolidated, can be represented as follows:

$$B = \begin{bmatrix} A_{hc} h_{c_{hc}}^{i} + K_{cp_i}^{1} & -K_{cp_i}^{1} & 0 & 0 \\ -K_{cp_i}^{j} & S_i^j I + K_{cp_i}^{j} + K_{ele_i}^{j} & -K_{ele_i}^{j} & 0 \\ 0 & -K_{ele_i}^{j} & -S_i^j I + K_{cp_i}^{j+1} + K_{ele_i}^{j} & -K_{cp_i}^{j+1} \\ 0 & 0 & -K_{cp_i}^{n+1} & A_{cc} h_{c_{cc}}^{i} + K_{cp_i}^{n+1} \end{bmatrix} (j = 1, 2, 3) \tag{9}$$

where the Seebeck coefficient of the thermoelement signifies the difference between the Seebeck coefficients of the P-type and N-type thermoelectric legs ($S = S_P - S_N$). Furthermore, the thermal conductance of each thermoelement K_{ele} is the summation of the thermal conductance of the P-type and N-type legs ($K_{ele} = \lambda_P A_P / l_P + \lambda_N A_N / l_N$).

The vectors T and C are expressed as:

$$T = \begin{bmatrix} T_{wh}(i) \\ T_{jh}^{j}(i) \\ T_{jc}^{j}(i) \\ T_{wc}(i) \end{bmatrix} (j = 1, 2, 3) \tag{10}$$

$$C = \begin{bmatrix} A_{hc} h_{c_{hc}}^{i} T_{fh}(i) \\ 0.5 I^2 R_i^j \\ 0.5 I^2 R_i^j \\ A_{cc} h_{c_{cc}}^{i} T_{fc}(i) \end{bmatrix} (j = 1, 2, 3) \tag{11}$$

The electric power output is the result of multiplying the load voltage by the current.

$$P_{TEG} = U_L \cdot I = \left\{ \sum_i \sum_j S_i^j \left[T_{jh}^{j}(i) - T_{jc}^{j}(i) \right] \right\}^2 R_L \bigg/ \left(R_L + \sum_i \sum_j R_i^j \right)^2 \tag{12}$$

where R_L denotes the electric resistance of the load and R signifies the internal resistance of the thermoelement.

The total electric power of the combined CBC-TEG power generation system is expressed as follows:

$$P_{tot} = P_{CBC} + P_{TEG} \tag{13}$$

3.2. Combustion Model

A quasi-one-dimensional model of the combustor is formulated to depict the process of supersonic combustion and heat dissipation. The central governing equations encompass the conservation of mass, conservation of momentum in the x-direction, equation of state, conservation equation for component i, and the conservation of energy pertinent to hydrocarbon fuel combustion, as presented below. It should be mentioned that considering the relatively high temperature and low pressure in the combustor, the ideal gas state equation is applied to describe the relationship among the density, pressure, and temperature of gas. For a comprehensive understanding of the detailed equations governing the supersonic combustion process, readers are referred to Ref. [32].

$$\frac{1}{\dot{m}_g} \frac{d\dot{m}_g}{dx} = \frac{1}{\rho_g} \frac{d\rho_g}{dx} + \frac{1}{u_g} \frac{du_g}{dx} + \frac{1}{A_{CD}} \frac{dA_{CD}}{dx} \tag{14}$$

$$\frac{1}{p_g}\frac{dp_g}{dx} + \frac{\gamma Ma^2}{u_g}\frac{du_g}{dx} + \frac{2\gamma Ma^2 C_f}{D_{h,CD}} + \frac{\gamma Ma^2(1-\psi)}{\dot{m}_g}\frac{d\dot{m}_g}{dx} = 0 \tag{15}$$

$$\frac{1}{p_g}\frac{dp_g}{dx} = \frac{1}{\rho_g}\frac{d\rho_g}{dx} + \frac{1}{T_g}\frac{dT_g}{dx} + \frac{1}{\overline{M}_W}\left[\overline{M}_W{}^2\left(\sum_i \frac{1}{M_{Wi}}\frac{dy_i}{dx}\right)\right] \tag{16}$$

$$\frac{dy_i}{dx} = \frac{\dot{\omega}_i M_{Wi}}{\rho_g u_g} + \frac{1}{\dot{m}_g}\frac{d\dot{m}_{i,add}}{dx} - \frac{y_i}{\dot{m}_g}\frac{d\dot{m}_g}{dx} \tag{17}$$

$$\frac{dh_g}{dx} = \frac{1}{\dot{m}_g}\frac{d\left[\sum_i h_{t,i}\dot{m}_i\right]_{add}}{dx} - \frac{q_w P_{w,CD}}{\dot{m}_g} - \frac{h_t}{\dot{m}_g}\frac{d\dot{m}_g}{dx} - u_g\frac{du_g}{dx} \tag{18}$$

3.3. Flow and Heat Transfer Model

The flow and heat transfer phenomena of the liquid metal within the wall cooling channels and the TEG heating channels, along with the hydrocarbon fuel within the TEG cooling channel, are described using a quasi-one-dimensional framework. This is done to align with the combustion model and to account for the temperature fluctuations along the flow direction within the TEG channels. The mass conservation principles for the coolants pertaining to the combustor wall and the thermoelectric generator can be articulated as follows:

$$\frac{1}{\rho_{cl}}\frac{d\rho_{cl}}{dx} + \frac{1}{u_{cl}}\frac{du_{cl}}{dx} + \frac{1}{A_{CC}}\frac{dA_{CC}}{dx} = 0 \tag{19}$$

The expression for the conservation of momentum in the horizontal direction (x-direction) applies to both liquid metal and fuel:

$$\dot{m}_{cl}\frac{du_{cl}}{dx} + A_{CC}\frac{dp_{cl}}{dx} + \frac{1}{2}\frac{C_f}{D_{h,CC}}\dot{m}_{cl}u_{cl} = 0 \tag{20}$$

where the friction loss factor (C_f) is calculated by the Colebrook equation:

$$\frac{1}{\sqrt{C_f}} = -2\lg\left(\frac{\Delta/D_r}{3.7} + \frac{2.51}{Re\sqrt{C_f}}\right) \tag{21}$$

where Δ/D_r is the relative roughness of channels.

The principle of energy conservation is represented by the following equation:

$$\frac{dh_{cl}}{dx} + u_{cl}\frac{du_{cl}}{dx} = \frac{q_w P_w}{\dot{m}_{cl}} \tag{22}$$

Recognizing the need to accurately depict the relationship between pressure, temperature, and density of hydrocarbon fuel and its cracking byproducts using a real gas state equation, this study employs the Redlich–Kwong and Peng–Robinson (RK-PR) state equation as a cubic equation of state, as detailed in Ref. [20].

$$\frac{dp_f}{dx} = \frac{d}{dx}\left[\frac{\rho_f R_u T_f}{\overline{M}_{wf} - b\rho_f} - \frac{a\alpha\left(T_f\right)\rho_f{}^2}{\left(\overline{M}_{wf} + \delta_1 b\rho_f\right)\left(\overline{M}_{wf} + \delta_2 b\rho_f\right)}\right] \tag{23}$$

Generally speaking, the pyrolysis process of hydrocarbon fuel is so complex that a mechanism model including thousands of step elementary reactions and hundreds of components becomes necessary to describe it accurately, which obviously needs a large number of computing resources. However, the demand on calculation accuracy is not very high in the cooling process of multi-stage TEG, and a two-step reaction model can basically meet the requirement. The overall reaction of n-dacane pyrolysis is given by:

$$\begin{aligned}C_{10}H_{22} \rightarrow\ & 0.119H_2 + 0.185CH_4 + 0.377C_2H_6 + 0.483C_2H_4 + 0.233C_3H_8 + 0.547C_3H_6 \\ & +0.086C_4H_{10} + 0.238C_4H_8 + 0.637C_7H_{14}\end{aligned} \tag{24}$$

where the pre-exponential factor of reaction is 5 × 10^{15} s^{-1}, the activation energy is set as 59,000 cal/mol, and the temperature coefficient is 0.

An overall reaction of n-heptane cracking is introduced to describe the pyrolysis of macromolecule products.

$$C_7H_{14} \rightarrow 0.7C_2H_4 + 0.7C_3H_6 + 0.875C_4H_8 \tag{25}$$

where the pre-exponential factor of reaction is 4 × 10^{15} s^{-1}, the activation energy is set as 61,000 cal/mol, and the temperature coefficient is also 0.

The calculation of the wall temperature in the cooling channels can be performed using the following formula:

$$T_{w,CC} = T_{cl} + \frac{q_w P_w}{h_c \eta_{fin} P_{w,CC}} \tag{26}$$

where η_{fin} represents the surface efficiency of the fins. The convection heat transfer coefficient is given by:

$$h_c = \frac{\lambda_{cl} Nu_{cl}}{D_{h,CC}} \tag{27}$$

As per the investigation conducted by Zhou [33], the Nusselt number for liquid sodium is expressed as follows:

$$Nu_{lm} = 4.82 + 0.0185Pe^{0.8} \tag{28}$$

The equation correlating heat transfer for hydrocarbon fuel and its cracking products, as presented in Ref. [34], is given by:

$$Nu_f = 0.027\mathrm{Re}_f{}^{0.8}\mathrm{Pr}_f{}^{0.33}\left(\frac{\mu_f}{\mu_w}\right)^{0.14} \tag{29}$$

where μ is the dynamic viscosity.

Given the substantial temperature gradient along the y-direction compared to that along the x-direction in Figure 1, the combustor wall temperature can be assessed through one-dimensional conduction. Consequently, the connection between the temperatures of the combustor wall and the wall cooling channel can be described as follows:

$$T_{w,CD} = T_{w,WC} + \frac{q_w \theta}{\lambda_w} \tag{30}$$

where θ is the thickness of combustor walls.

3.4. Calculation Flowchart and Input Parameters

The flowchart detailing the computation process for the integrated CBC-TEG power generation system connected with a scramjet is depicted in Figure 2. Upon deriving the mass flowrate of hydrocarbon fuel based on flight conditions and the fuel equivalence ratio, a three-step iteration is employed to optimize the CBC power output. This calculation based on the optimization algorithm [35] involves adjusting the compression ratio, the effectiveness of recuperation, and the temperature differentials between the hot and cold ends of the precooler. A comprehensive depiction of the calculation procedure for power optimization in a simple recuperated CBC system with a finite cold source has been introduced in Ref. [24]. Subsequently, the supersonic combustion process is simulated utilizing a quasi-one-dimensional combustion model, accounting for initial fuel injection temperature and liquid metal mass flowrate, in order to provide relevant flow field parameters within the combustor. Employing the Eckert Reference Enthalpy method to calculate the heat flux on the combustor walls, a simulation of the wall cooling process is conducted to ascertain the outlet temperature of the wall cooling channels, which directly corresponds to the inlet temperature of the liquid metal in the CBC heater (T_{lm2}). Following this, the thermoelectric generator's performance is evaluated through coupled calculations involving the thermoelectric module and the heating and cooling channels of the TEG, utilizing both the fuel outlet temperature from the precooler (T_{f2}) and T_{lm2} as input variables. The outlet temperature of the TEG cooling channel (T_{f3}) influences fuel injection conditions and consequently impacts the combustion process. Thus, an iterative process is imperative to ensure energy conservation among the combustor, the wall cooling channels, and the combined CBC-TEG power generation system. Subsequent to achieving energy conservation, another iteration is implemented, adjusting the liquid metal mass flowrate until the TEG heating channel outlet temperature (T_{lm4}) matches the inlet temperature of the wall cooling channel (T_{lm1}). Ultimately, the comprehensive performance parameters of the CBC-TEG system, encompassing total electric power, CBC power, and TEG power, are determined through multiple iterative cycles.

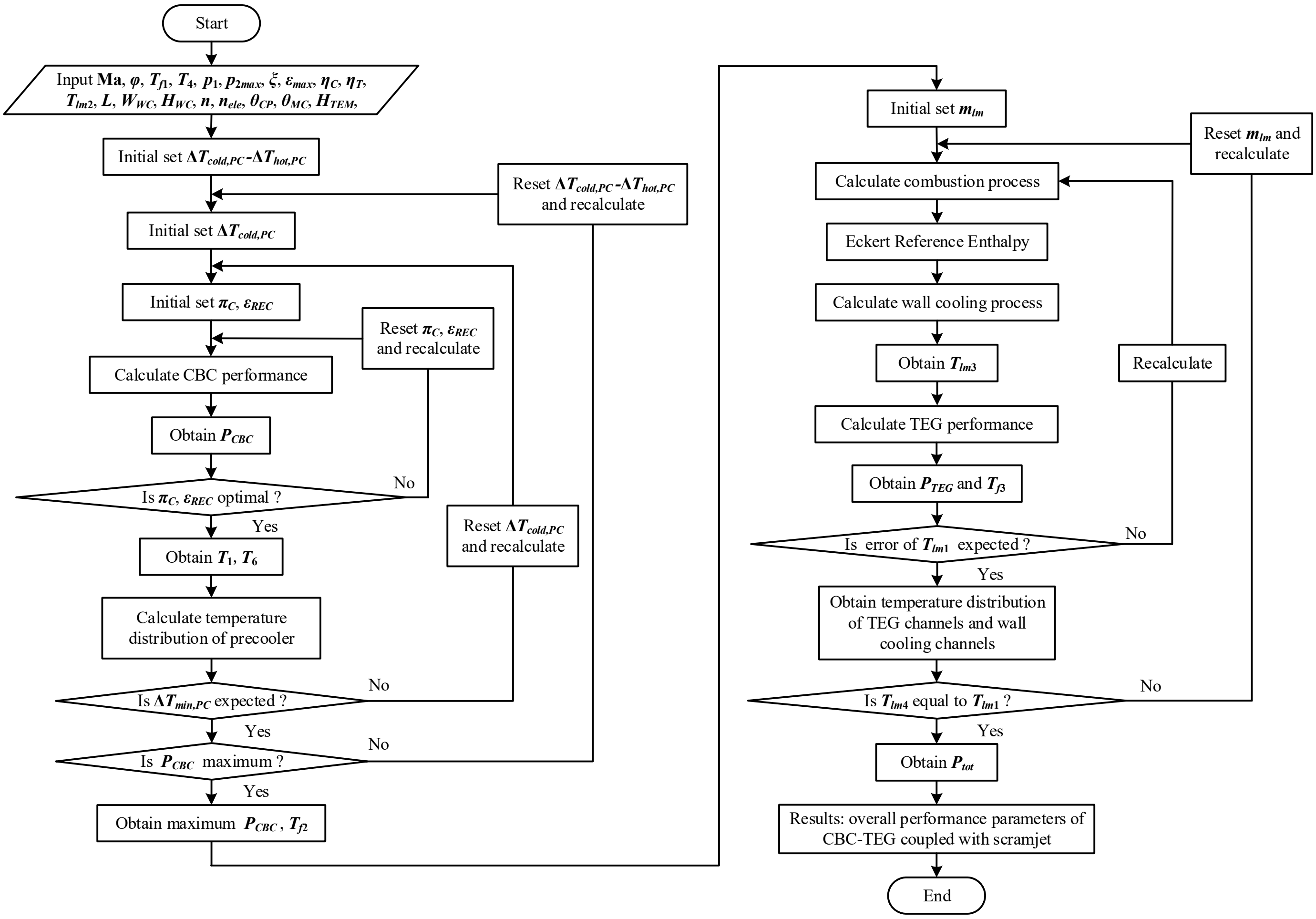

Figure 2. Calculation flowchart.

The input parameters for the CBC-TEG system are outlined in Table 1. To ensure operational safety, the upper temperature limit for the liquid metal is designated as 1150 K, taking into consideration that the boiling point of liquid sodium is approximately 1156 K. The parameters pertaining to the supercritical carbon dioxide closed-Brayton-cycle are extracted from Ref. [24]. Considering the extremely high cycle pressure for S-CO_2 CBC (the highest pressure is over 30 MPa in this study) makes it difficult to avoid working fluid leakage at high temperatures, a fixed turbine inlet temperature of 823.15 K (550 °C) is employed rather than a value varied with liquid metal temperature [36]. In this analysis, the number of stages for the thermoelectric modules (TEM) is determined to be 3 rather than 4, primarily due to the relatively constrained available temperature difference for TEM. Furthermore, a singular type of thermoelectric material, specifically cubic $AgPb_mTe_{2+m}$, is employed in this study. This material is chosen for its favorable behavior in terms of the thermoelectric figure of merit (ZT) within the intermediate temperature range (roughly 500 K to 800 K). Corresponding thermoelectric material parameters, including the Seebeck coefficient, thermal conductance, and electrical conductivity, come from Ref. [37]. This temperature range closely aligns with that of the thermoelectric generator operating within the combined CBC-TEG power generation system.

Table 1. Basic input parameters of CBC-TEG.

Parameter	Value
Maximum temperature of liquid metal	1150 K
Inlet temperature of fuel	300 K
Fuel inlet pressure	3 MPa
Generator efficiency	0.92
Turbine inlet temperature	823.15 K
Minimum temperature difference in primary cooler	5 K
Compressor inlet pressure	7.4 MPa
Upper limit of highest cycle pressure	35 MPa
Relative pressure loss coefficient of heat-exchanger	0.02
Compressor isentropic efficiency	0.89
Turbine isentropic efficiency	0.93
Maximum effectiveness of heat-exchanger	0.95
Stage number of TEM	3
Total height of TEM	0.04 m
Channel height	0.002 m
Channel width	0.002 m
Thermoelement gap	0.0004 m
Metallic connector thickness	0.0001 m

The dimensional characteristics of the combustor duct and the wall cooling channels are visualized in Figure 3. Specifically, the combustor duct comprises a 0.5 m long section with dimensions of 0.04 m (width) by 0.1 m (height). This is succeeded by a 0.7 m long segment featuring an approximate divergence of the duct floor at an angle of 1.6 degrees. Conversely, the geometry of the wall cooling channel is defined by dimensions of 1.2 m in length, 0.001 m in width, and 0.002 m in height. The fins integrated within the channel have a thickness of 0.001 m.

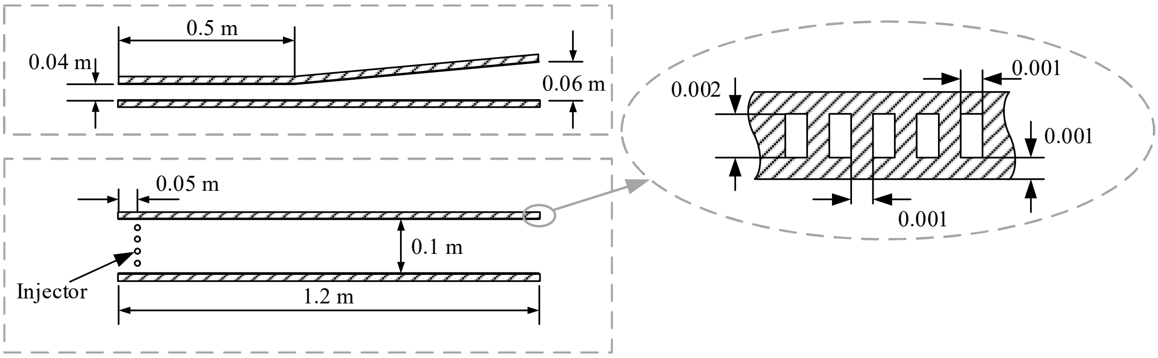

Figure 3. Geometric configuration of hydrocarbon-fueled scramjet combustor with wall cooling channel.

4. Results and Analysis

4.1. Model Validation of Scramjet Combustor

The validation of the hydrocarbon fuel combustion process model is carried out through comparison with experimental data collected from the HIT direct connect scramjet platform. The physical configuration of this platform is depicted in Figure 4. Notably, the width of the combustor within the platform is specified as 0.1 m. The introduction of hydrocarbon fuel into the combustor is facilitated by means of a strut. It is worth mentioning that due to the absence of an effective cooling system, the operational duration of the scramjet platform is limited, thus constraining its sustained operation.

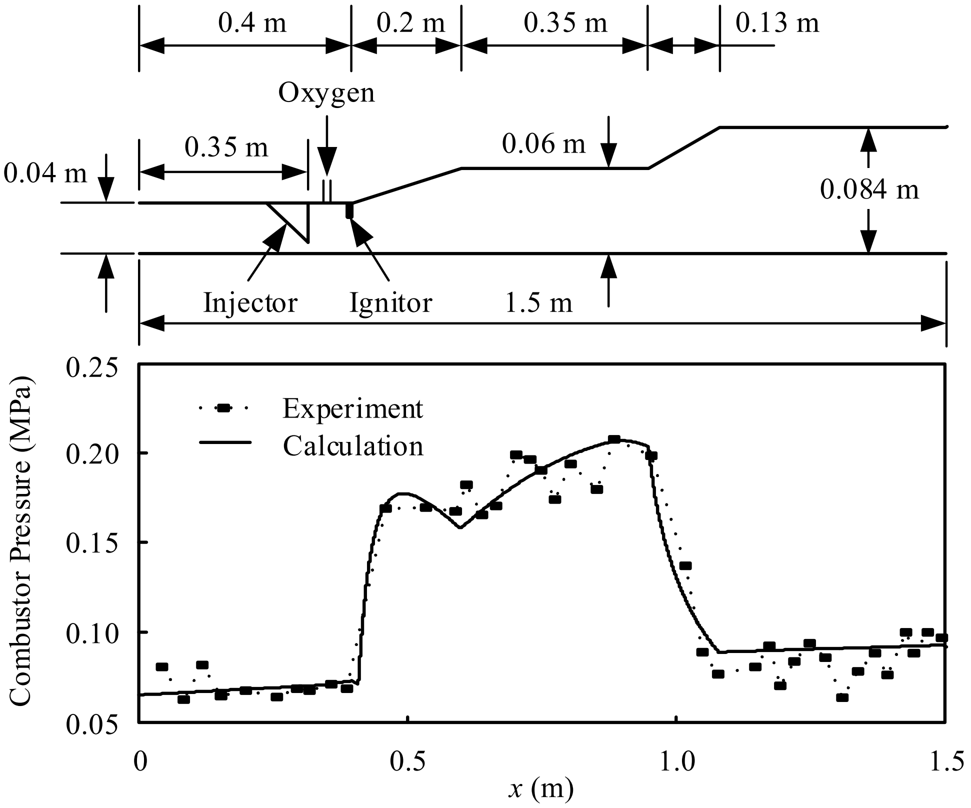

Figure 4. Combustion model validation based on HIT scramjet experimental data.

The static pressure within the combustor was measured utilizing pressure sensors located at pressure holes integrated into the combustor walls. The current signal, operating within the range of 4–20 mA, was gathered by the C-RIO system from National Instruments Corporation. The data acquisition was conducted at a frequency of 500 Hz, with a natural frequency response of 50 kHz. Notably, the temperature drift remains below 0.05%, and both the repeatability error and nonlinearity error, in conjunction with the comprehensive error of the full-scale range, are held within a range of ±0.1%. For the purpose of simulating the flight conditions corresponding to a Mach number of 7, the inlet parameters for the combustor were established. Specifically, the Mach number, static pressure, and static temperature at the combustor inlet were set to 2.8, 65 kPa, and 726 K, respectively. Furthermore, the fuel equivalence ratio was approximately 0.56. It is essential to note that due to limitations in the heating capacity of the platform, the inlet total temperature was lower than the expected value for Mach 7 conditions. To facilitate the swift ignition of hydrocarbon fuel, a minor quantity of oxygen and plasma, generated by ionizing nitrogen, were introduced downstream of the strut injector to assist the ignition process.

In the calculations, n-decane is assumed as the only component of the hydrocarbon fuel. The combustor wall temperature is set at 900 K. A comparison between the experimental data and the calculation results reveals that the quasi-one-dimensional combustor model can offer an approximate description of the supersonic combustion process. In the initial duct segment devoid of combustion, the model effectively simulates the airflow process, with the exception of the impact of the oblique shock wave at the platform inlet. Within the first divergent section, the model approximates the pressure surge generated by combustion. However, the pressure fluctuations during the supersonic combustion process, primarily driven by the interaction between shock waves and boundary layers, cannot be effectively captured by the simplified mixing model and reaction mechanism inherent to the quasi-one-dimensional approach. Fortunately, in this study, the combustion model serves primarily to furnish the mainstream combustor parameters required for calculating wall heat flux via the Eckert Reference Enthalpy Method. The intricate interaction between shock waves and boundary layers is not the focal point of investigation. In comparison to a more intricate simulation involving a complex three-dimensional computational fluid dynamics (CFD) model, the rapid computations offered by the quasi-one-dimensional combustion model hold more significance given the numerous iterations within the combined system model. In summary, the quasi-one-dimensional combustion model manages to replicate the static pressure distribution observed in the experimental process and proves to be applicable for simulating combustion heat dissipation.

4.2. Effect of Fuel Equivalent Ratio

Variations in power generation parameters with respect to fuel equivalence ratio at different Mach numbers are illustrated in Figure 5. It is obvious that at a constant flight Mach number, the mass flowrate of air remains consistent. However, the mass flowrate of fuel as well as the corresponding cooling capacity of the fuel utilized by the combined CBC-TEG power generation system increase proportionally with the fuel equivalence ratio. This trend contributes to an enhanced electric power output, as observed in Figure 5a. This power increase can be attributed to the amplified CBC power. Surprisingly, the TEG power actually decreases with the elevation of the fuel equivalence ratio, as shown in Figure 5b. This phenomenon is explained by the fact that the higher temperature of the liquid metal leads to a greater heat release within the CBC heater, redirecting heat from the TEG's heating channels. To be specific, with a greater cooling capacity of the fuel, the power generation process demands an augmented heat input. Following the reference enthalpy method, the inlet temperature of the wall cooling channel must decrease to augment heat dissipation from the gas to the walls, resulting in a reduction of the liquid metal's mass flowrate. Consequently, the outlet temperature of the CBC heater, which corresponds to the inlet temperature of the TEG's heating channel, needs to decrease rapidly to maintain a substantial specific enthalpy difference within the heater. This behavior is depicted in Figure 5c. Consequently, the outlet temperature of the TEG's heating channel experiences a decrease in line with the increment of the fuel equivalence ratio. This lowering of temperature is crucial to provide the required heat input for the thermoelectric modules (TEM), as illustrated in Figure 5d.

Consequently, the temperature of the liquid metal within the TEG's heating channel diminishes in response to a rise in the fuel equivalence ratio, as shown in Figure 6. This decrease in temperature leads to a reduction in the available temperature difference. Consequently, the conversion efficiency of the TEG experiences a substantial decline with increasing φ, as illustrated in Figure 5f. In parallel, the heat transfer rate from the liquid metal to the thermoelectric modules (TEM) in the TEG's heating channel undergoes only minor changes, as indicated in Figure 5e. Considering the interplay between conversion efficiency and heat transfer rate within the heating channel, the electric power output of the thermoelectric generator contracts at higher fuel equivalence ratios. This observation underscores the pivotal role of the fuel equivalence ratio in influencing the power distribution of the CBC-TEG system. Furthermore, the amplification effect on power from the TEG is more pronounced at lower φ values.

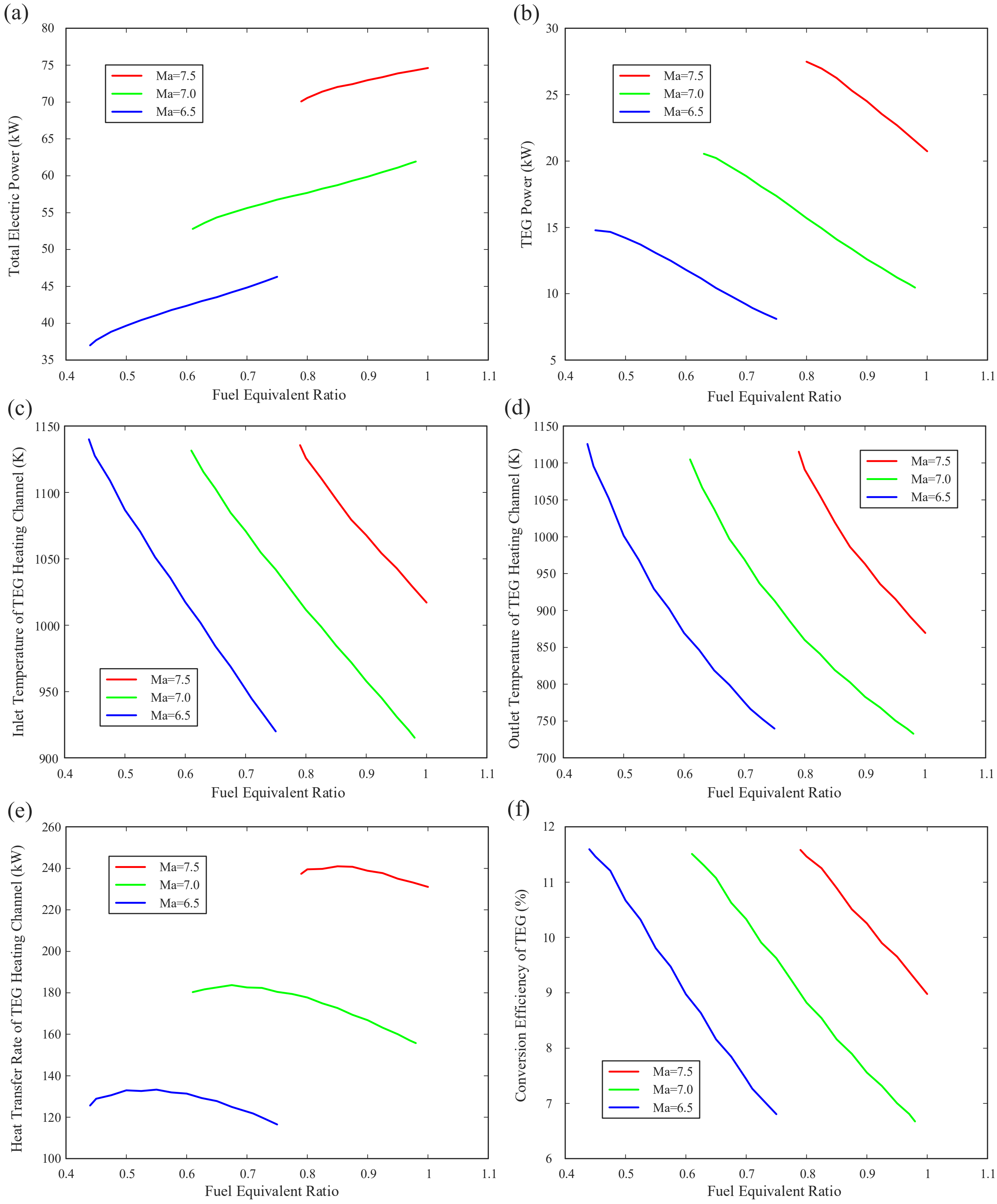

Figure 5. Parameter variation with φ at different Ma: (**a**) P_{tot}; (**b**) P_{TEG}; (**c**) inlet temperature of TEG heating channel; (**d**) outlet temperature of TEG heating channel; (**e**) heat transfer rate of TEG heating channel; (**f**) TEG conversion efficiency.

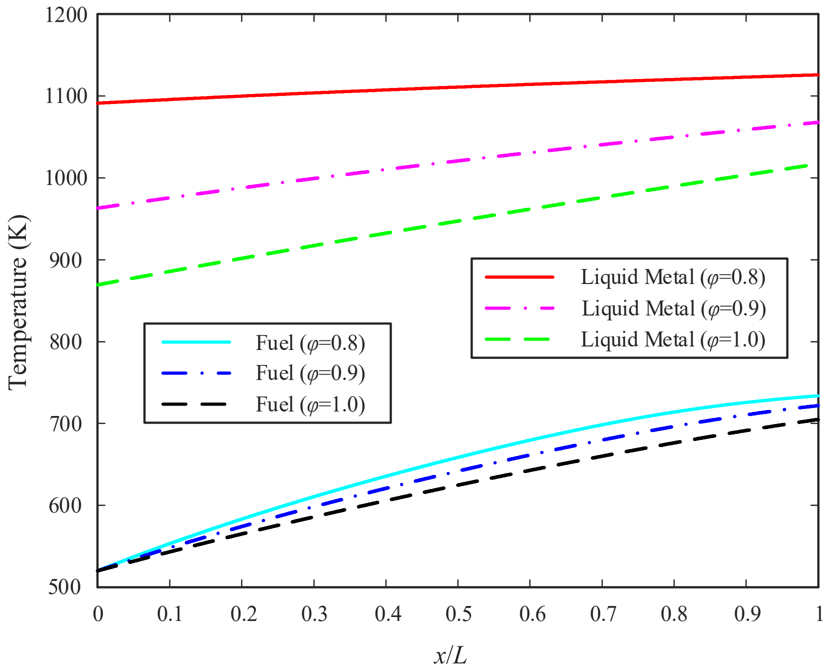

Figure 6. Temperature distributions of TEG heating and cooling channels with different φ (Ma = 7.5).

Note that the heat transfer rate in TEG heating channel, which depends on the product of the mass flowrate and specific enthalpy difference of liquid metal, increases with φ firstly and then decreases. It is mainly caused by the reduction of mass flowrate and the improvement of specific enthalpy difference for liquid metal. In the view of energy conservation, TEG requires less heat input when its conversion efficiency is lower at higher φ, leading to the decrease of the heat transfer rate in TEG heating channel.

4.3. Operating Range and Performance Boundary of CBC-TEG

The predicted working envelope and corresponding performance boundary of the combined CBC-TEG power generation system are illustrated in Figure 7. Maintaining a constant flight Mach number, it becomes evident that the system's operation is constrained within specific ranges of fuel equivalence ratios. Within this context, there exist three primary limitations that dictate the operation of the CBC-TEG system. The initial limitation arises from the need to ensure that the fuel equivalence ratio remains below 1. This precaution is taken to prevent scenarios where a portion of the fuel must be abandoned due to inadequate combustion. The second constraint relates to the temperature gradient of the thermoelectric generator (TEG). The efficiency of the TEG's thermoelectric conversion and the heat transfer between the TEG's heating and cooling channels are contingent upon the temperature gradient of the thermoelectric modules (TEM). Therefore, the temperature within the TEG's heating channel must surpass the corresponding fuel temperature within the TEG's cooling channel. As discussed in Section 4.2, the outlet temperature of the TEG's heating channel decreases with an increase in the fuel equivalence ratio. Consequently, when φ reaches sufficiently high levels, the outlet temperature of the TEG's heating channel aligns with the inlet temperature of the TEG's cooling channel. This value then establishes an upper limit for the fuel equivalence ratio. The third limitation originates from the heat dissipation occurring on the combustor walls. Following principles of energy conservation, the heat dissipation capacity of the walls is equivalent to the sum of the heat absorption capacity of the hydrocarbon fuel and the electric power generated by the CBC-TEG system. Although the heat dissipation from combustion can be manipulated by adjusting the liquid metal mass flowrate to modify the temperature distribution across the combustor walls, a lower limit for gas-to-wall heat dissipation remains. In situations where nearly all wall cooling channels function at the maximum liquid metal temperature, the mass flowrate of the liquid metal approaches infinity, thereby hindering the achievement of energy conservation. This sets a lower threshold for the fuel equivalence ratio, under which the energy conservation cannot be upheld.

Consequently, the working envelope of the combined CBC-TEG power generation system consists of three boundary lines. When the flight Mach number is relatively low, the heat dissipation into combustor walls is relatively few, and the according lower limit of fuel equivalence ratio is also lower. Meanwhile, the thermoelectric generator will not work if the fuel equivalence ratio is over its upper limit, considering the liquid metal outlet temperature in the TEG heating channel must be higher than the fuel inlet temperature of the TEG cooling channel. With increased flight Mach number, the thermal loading of airflow becomes larger, leading to a greater heat exchange intensity from gas to combustor walls. The demand on the cooling capacity of fuel improves with the increased combustion dissipation, causing a larger lower limit of fuel equivalence ratio. Finally, a curve–curve intersection of heat dissipation limit and fuel equivalence limit occurs, and the according Mach number is the maximum value for CBC-TEG operation.

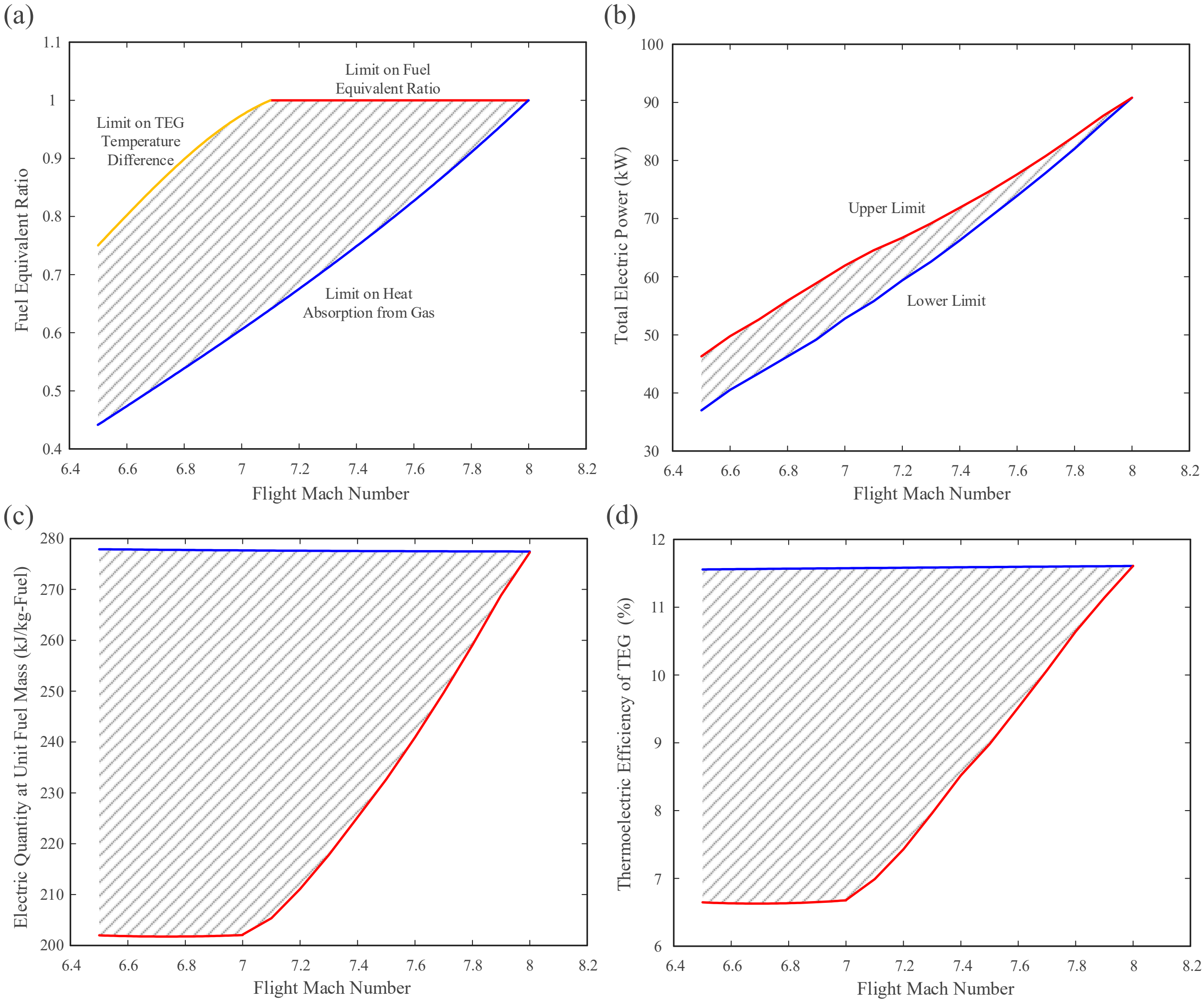

Figure 7. *Cont.*

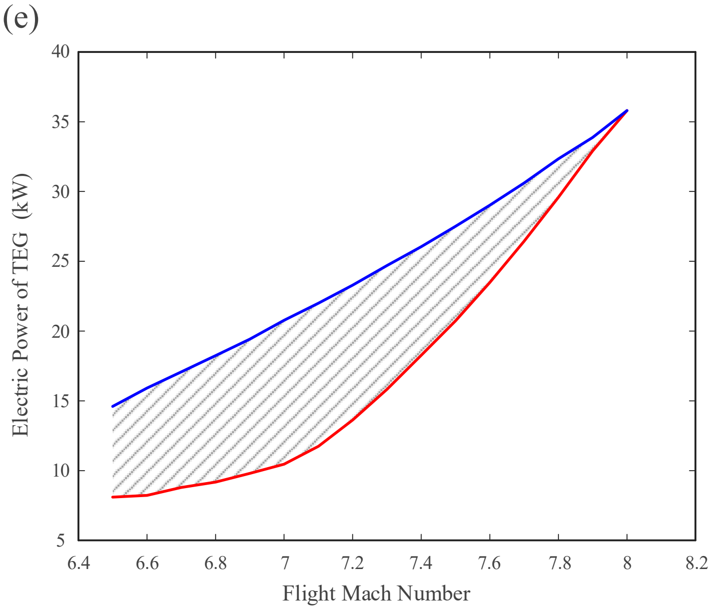

Figure 7. Performance boundary of combined CBC-TEG power generation system: (**a**) working envelope; (**b**) total electric power; (**c**) electric quantity at unit fuel mass; (**d**) TEG efficiency; (**e**) TEG power.

As a result of these constraints, the achievable total power spectrum of the combined CBC-TEG power generation system forms an approximate triangular shape, as shown in Figure 7b. The total power output of the CBC-TEG system can be manipulated by altering the fuel equivalence ratio, especially at lower flight Mach numbers. However, as the flight Mach numbers increase, the range of viable fuel equivalence ratios diminishes and eventually disappears. Note that the total power of the combined power generation system is relatively low (40–90 kW), but it does not indicate the actual power generation capacity of CBC-TEG. In fact, it is mainly caused by the relatively low-level thrust of the coupled scramjet. Under the finite cold source condition, the electric quantity at unit fuel mass is a more suitable parameter to measure the power generation capacity.

As illustrated in Figure 7c, the peak value of electric output per unit of fuel mass corresponds to the minimum fuel equivalence ratio. This phenomenon is primarily caused by the highest achievable thermoelectric conversion efficiency and according TEG power, as shown in Figure 7d,e. In alignment with the discussion in Section 4.3, a reduced fuel equivalence ratio leads to an increase in the liquid metal mass flowrate, consequently elevating the temperature within the TEG's heating channels and augmenting the associated temperature differences, as demonstrated in Figure 6. Following the Seebeck effect, a larger temperature difference contributes positively to enhancing the thermoelectric conversion efficiency. Furthermore, the maximum value of the electric quantity at unit fuel mass reaches 277.0 kJ/kg, which is about 33.4% higher than the according CBC power of 207.6 kJ/kg. That is, the combined CBC-TEG power generation system brings a significant power improvement when it is coupled with hydrocarbon-fueled scramjet on a hypersonic vehicle with finite cold source.

It should be noted that the model of the combined CBC-TEG power generation system in this paper can hardly reflect the actual performance boundary, considering the mixing model of supersonic combustion process utilized by this article is more suitable for a single flight Mach number, rather than Mach numbers ranging from 6.5 to 8.0. In fact, this work is aimed to exhibit the performance variation and limits of the combined CBC-TEG power generation system on hypersonic vehicles qualitatively, rather than a quantitative analysis.

5. Conclusions

This study offers a comprehensive performance evaluation of the combined CBC-TEG power generation system integrated with a hydrocarbon-fueled scramjet. The analysis for the effect of fuel equivalent ratio on power generation at different flight Mach numbers has been performed, and the operating characteristics and performance limits have been exhibited. The main conclusions are summed up as follows:

1. Due to the larger fuel cooling capacity utilized by the combined CBC-TEG power generation system, the increase of fuel equivalence ratio leads to a higher total electric power and a higher CBC power but a lower TEG power at a constant flight Mach number.
2. There are three limits on the fuel equivalence ratio, TEG temperature difference, and heat dissipation adjustment for the operation of the CBC-TEG system.
3. The total power of CBC-TEG can be adjusted through changing the fuel equivalence ratio, but the adjustable range becomes smaller with the increased Mach number.
4. The maximum value of the electric quantity at unit fuel mass for CBC-TEG reaches 277.0 kJ/kg, which is about 33.4% higher than that of the standalone CBC system at 207.6 kJ/kg.

This article exhibits the theoretical performance of the combined CBC-TEG power generation system coupled with hydrocarbon-fueled scramjet and its operation limits on hypersonic vehicles.

6. Future Work

In our future works, a comprehensive 3D simulation and structural analysis of the three-stage TEG designed for the CBC-TEG system will be performed. Furthermore, an experimental TEG system will be established in which the thermoelectric module is heated by liquid metal and cooled by hydrocarbon fuel to facilitate practical engineering applications.

Author Contributions: Conceptualization, K.C. and J.Q.; methodology, K.C.; software, W.J.; validation, K.C. and J.L.; investigation, K.C.; writing—original draft preparation, K.C. and W.J.; writing—review and editing, K.C. and J.L. All authors have read and agreed to the published version of the manuscript.

Funding: This research was funded by National Natural Science Foundation of China, grant numbers 52006044 and 52076051.

Conflicts of Interest: The authors declare no conflict of interest.

References

1. Viviani, A.; Aprovitola, A.; Pezzella, G.; Rainone, C. CFD design capabilities for next generation high-speed aircraft. *Acta Astronaut.* **2021**, *178*, 143–158. [CrossRef]
2. Zhang, T.; Yan, X.; Huang, W.; Che, X.; Wang, Z.; Lu, E. Design and analysis of the air-breathing aircraft with the full-body wave-ride performance. *Aerosp. Sci. Technol.* **2021**, *119*, 107133. [CrossRef]
3. Huang, W.; Du, Z.; Yan, L.; Moradi, R. Flame propagation and stabilization in dual-mode scramjet combustors: A survey. *Prog. Aerosp. Sci.* **2018**, *101*, 13–30. [CrossRef]
4. Huang, W.; Du, Z.; Yan, L.; Xia, Z. Supersonic mixing in airbreathing propulsion systems for hypersonic flights. *Prog. Aerosp. Sci.* **2019**, *109*, 100545. [CrossRef]
5. Tian, Y.; Shi, W.; Guo, M.; Liu, Y.; Zhang, C.; Le, J. Investigation of combustion characteristics in a hydrogen-fueled scramjet combustor. *Acta Astronaut.* **2021**, *186*, 486–495. [CrossRef]
6. Li, N. Response of shock train to fluctuating angle of attack in a scramjet inlet-isolator. *Acta Astronaut.* **2022**, *190*, 430–443. [CrossRef]
7. Zhang, T.; Wang, Z.; Huang, W.; Ingham, D.; Ma, L.; Porkashanian, M. An analysis tool of the rocket-based combined cycle engine and its appilication in the two-stage-to-orbit mission. *Energy* **2020**, *193*, 116709. [CrossRef]
8. Zhang, T.; Yan, X.; Huang, W.; Che, X.; Wang, Z. Multidisciplinary design optimization of a wide speed range vehicle with waveride airframe and RBCC engine. *Energy* **2021**, *235*, 121386. [CrossRef]
9. Zheng, J.; Chang, J.; Ma, J.; Yu, D. Modeling and analysis of windmilling operation during mode transition of a turbine-based-combined cycle engine. *Aerosp. Sci. Technol.* **2021**, *109*, 106423. [CrossRef]

10. Jing, T.; Xu, Z.; Xu, J.; Qin, F.; He, G.; Liu, B. Characteristics of gaseous film cooling with hydrocarbon fuel in supersonic combustion chamber. *Acta Astronaut.* **2022**, *190*, 74–82. [CrossRef]
11. Yu, X.; Wang, C.; Yu, D. Precooler-design & engine-performance conjugated optimization for fuel direct precooled airbreathing propulsion. *Energy* **2019**, *170*, 546–556.
12. Xi, Y.; Meng, Y. Adaptive actuator failure compensation control for hypersonic vehicle with full state constraints. *Aerosp. Sci. Technol.* **2019**, *85*, 464–473. [CrossRef]
13. Zhang, D.; Qin, J.; Feng, Y.; Ren, F.; Bao, W. Performance evaluation of power generation system with fuel vapor turbine onboard hydrocarbon fueled scramjets. *Energy* **2014**, *77*, 732–741. [CrossRef]
14. Song, S.; Liu, W.; Peitsch, D.; Schaefer, U. Detailed Design of a high speed switched reluctance starter/generator for more/all electric aircraft. *Chin. J. Aeronaut.* **2010**, *23*, 216–226.
15. Sforza, P.M. Electric power generation onboard hypersonic aircraft. In Proceedings of the 45th AIAA/ASME/SAE/ASEE Joint Propulsion Conference & Exhibit, Denver, CO, USA, 1–4 August 2009.
16. Zhang, Y.; Wang, L.; Wang, S.; Wang, P.; Liao, H.; Peng, Y. Auxiliary power unit failure prediction using quantified generalized renewal process. *Microelectron. Reliab.* **2018**, *84*, 215–225. [CrossRef]
17. Surhone, L.M.; Tennoe, M.T.; Henssonow, S.F. *Ram Air Turbine*; Betascript Publishing: Beau Bassin, Mauritius, 2010.
18. MacHeret, S.O.; Shneider, M.N.; Miles, R.B. Magnetohydrodynamic power extraction from cold hypersonic airflows with external ionizers. *J. Propuls. Power* **2002**, *18*, 424–431. [CrossRef]
19. Harada, N.; Kikuchi, T.; Lineberry, J.T. Numerical simulation for hypersonic vehicle onboard magnetohydrodynamic power generation. In Proceedings of the Conference Numerical Simulation for Hypersonic Vehicle Onboard Magnetohydrodynamic Power Generation, Johor Baharu, Malaysia, 1–3 December 2008.
20. Li, H.; Qin, J.; Jiang, Y.; Zhang, D.; Cheng, K.; Bao, W.; Huang, H. Experimental and theoretical investigation of power generation scheme driven by thermal cracked gaseous hydrocarbon fuel for hypersonic vehicle. *Energy Convers. Manag.* **2018**, *165*, 334–343. [CrossRef]
21. Zhang, R.; Guo, K.; Wang, C.; Zhang, D.; Tian, W.; Qiu, S.; Su, G.H.; Deng, J. Thermal-hydraulic analysis of gas-cooled space nuclear reactor power system with closed Brayton cycle. *Int. J. Energy Res.* **2021**, *45*, 11851–11867. [CrossRef]
22. Sánchez, D.; Muñoz de Escalona, J.M.; Chacartegui, R.; Muñoz, A.; Sánchez, T. A comparison between molten carbonate fuel cells based hybrid systems using air and supercritical carbon dioxide Brayton cycles with state of the art technology. *J. Power Sources* **2011**, *196*, 4347–4354. [CrossRef]
23. Kim, S.; Kim, M.S.; Kim, M. Parametric study and optimization of closed Brayton power cycle considering the charge amount of working fluid. *Energy* **2020**, *198*, 117353. [CrossRef]
24. Cheng, K.; Qin, J.; Sun, H.; Li, H.; He, S.; Zhang, S.; Bao, W. Power optimization and comparison between simple recuperated and recompressing supercritical carbon dioxide closed-Brayton-cycle with finite cold source on hypersonic vehicles. *Energy* **2019**, *181*, 1189–1201. [CrossRef]
25. Yazawa, K.; Shakouri, A. Fuel-burning thermoelectric generators for the future of electric vehicles. *Energy Convers. Manag.* **2021**, *227*, 113523. [CrossRef]
26. Maduabuchi, C.C.; Lamba, R.; Eke, M.; Ejiogu, E. Multi-dimensional optimization of a concentrated solar thermoelectric generator. *Int. J. Energy Res.* **2021**, *46*, 5896–5907. [CrossRef]
27. Zhang, C.; Shu, G.; Tian, H.; Wei, H.; Liang, X. Comparative study of alternative ORC-based combined power systems to exploit high temperature waste heat. *Energy Convers. Manag.* **2015**, *89*, 541–554. [CrossRef]
28. Feng, Y.; Cai, W.; Wang, S.; Zhang, C.; Liu, Y. Numerical evaluation of energy system based on Fresnel concentrating solar collector, Stirling engine, and thermoelectric generator with electrical energy storage. *Int. J. Energy Res.* **2021**, *45*, 19423–19438. [CrossRef]
29. Guo, X.; Zhang, H.; Guo, Y.; Wang, J. A novel triple-cycle system based on high-temperature proton exchange membrane fuel cell, thermoelectric generator, and thermally regenerative electrochemical refrigerator for power and cooling cogeneration. *Int. J. Energy Res.* **2022**, *46*, 7529–7541. [CrossRef]
30. Cheng, K.; Qin, J.; Sun, H.; Dang, C.; Zhang, S.; Liu, X.; Bao, W. Performance assessment of an integrated power generation and refrigeration system on hypersonic vehicles. *Aerosp. Sci. Technol.* **2019**, *89*, 192–203. [CrossRef]
31. Tahaeri, B.; Jabari, F.; Foroud, A.A. A green cogeneration microgrid composed of water-source heat pumps, a gravity energy storage, and a bio-fueled gas turbine: Design and techno-economic optimization. *Sustain. Cities Soc.* **2023**, *95*, 104594. [CrossRef]
32. Xiong, Y.; Qin, J.; Cheng, K.; Zhang, S.; Feng, Y. Quasi-one-dimensional model of hydrocarbon-fueled scramjet combustor coupled with regenerative cooling. *Int. J. Aerosp. Eng.* **2022**, *2022*, 9931498. [CrossRef]
33. Zhou, C.; Huber, K.; Cheng, X. Validation of the modified ATHLET code with the natural convection test of the PHENIX reactor. *Ann. Nucl. Energy* **2013**, *59*, 31–46. [CrossRef]
34. Li, X.; Huai, X.; Cai, J.; Zhong, F.; Fan, X.; Guo, Z. Convective heat transfer characteristics of China RP-3 aviation kerosene at supercritical pressure. *Appl. Therm. Eng.* **2011**, *31*, 2360–2366. [CrossRef]
35. Taheri, B.; Aghajani, G.; Sedaghat, M. Economic dispatch in a power system considering environmental pollution using a multi-objective particle swarm optimization algorithm based on the Pareto criterion and fuzzy logic. *Int. J. Energy Environ. Eng.* **2017**, *8*, 99–107. [CrossRef]

36. Dostal, V.; Driscoll, M.J.; Hejzlar, P. *A Supercritical Carbon Dioxide Cycle for Next Generation Nuclear Reactors, MIT-ANP-TR-100*; Massachusetts Institute of Technology: Cambridge, MA, USA, 2004.
37. Hsu, K.F.; Loo, S.; Guo, F.; Chen, W.; Dyck, J.S.; Uher, C.; Hogan, T.; Polychroniadis, E.K.; Kanatzidis, M.G. Cubic $AgPb_mSbTe_{2+m}$: Bulk thermoelectric materials with high figure of merit. *Science* **2004**, *303*, 818–821. [CrossRef] [PubMed]